AIR TEMPERATURE ANALYSIS AND CONTROL IMPROVEMENT FOR THE STORAGE RING TUNNEL

Jui-Chi Chang[a], June-Rong Chen[a,b], Zong-Da Tsai[a], Ming-Tsun Ke[c]
[a]National Synchrotron Radiation Research Center, Hsinchu, Taiwan
[b] Department of Atomic Science, National Tsing-Hua University, Hsinchu, Taiwan
[c] Department of Air-Conditioning and Refrigeration Engineering, National Taipei University of Technology, Taipei 106, Taiwan

Abstract

The stability of the electron beam orbit had been observed to be sensitive to the utility conditions. The stability of air temperature in the storage ring tunnel is one of the most critical factors. Accordingly, a series of air conditioning system upgrade studies and projects have been conducted at the Taiwan Light Source (TLS). Computational fluid dynamics (CFD) is applied to simulate the flow field and the spatial temperature distribution in the storage ring tunnel. The circumference and the height of the storage ring tunnel are 120m and 2.8m, respectively. The temperature data and the flow rates at different locations around the storage ring tunnel are collected as the boundary conditions. The k-ε turbulence model is applied to simulate the flow field in the three dimensional space. The global air temperature variation related to time in the storage ring tunnel is currently controlled within $\pm 0.1^{o}$C. However, the temperature difference between two different locations is as high as 2^{o}C. Some measures improving the temperature uniformity will be taken according to the CFD simulated results.

INTRODUCTION

The TLS has made studied the utility effect on beam quality [1] [2] to verify the thermal effects on the stability of the electron beam orbit. The propagation routes from the temperature variation to the beam quality are also illustrated. Accordingly, we have improved the air conditioning (A/C) system of the storage ring tunnel [3] and analyzed the flow field and temperature distribution of the two dimensional magnet lattice girder [4] and the three dimensional experimental hall [5] through CFD simulation. Although the air temperature variation along the time in the storage ring tunnel is globally controlled within $\pm 1^{o}$C currently, the temperature difference between different locations is as high as 2-3 ^{o}C. To cope with the spatial temperature difference problem, the three dimensional flow field and temperature distribution inside the storage ring tunnel are simulated by using FLUENT 6.1, a commercial CFD software. The physical three dimensional model of the storage ring tunnel is built by using GAMBIT, an integrated pre-processing software.

The modelling and the simulation analysis procedure are described as follows.

1. Set up the physical shapes, sizes and boundary condition according to the actual measurement.
2. Generate adequate grids according to the model shape and set the corresponding boundary and initial conditions.
3. Choose the computation model and set the boundary conditions. The k-ε turbulence model is applied to the simulation.
4. Check if the computation results converge. If yes, then conduct the post-processing to draw the flow field and the temperature distribution.

There are some assumptions are made to simplify the computation. The simulation is assumed as a three dimensional steady, viscous, incompressible problem.

GEOMETRY MODELING AND BOUNDARY CONDITIONS

The geometric model of the storage ring tunnel with 120m circumference and 2.8m height is precisely set up. There are 16 supplied air exits and 8 air exhausts are also distributed in the 3D model according to the actual locations and sizes. The heat sources along the storage ring tunnel, including bending magnets, quadrupole magnets, sextupole magnets, insertion devices, radio frequency chambers and the cables overhead are all built in the model. Although the shapes of those heat sources are simplified and some trivial piping system and small apparatuses are neglected, the simulated results would not be affected too much. More than three hundred thousand tetrahedron grids are generated in the simulated area. The grid structure of the simulation model is shown in Figure 1. The blue and red rectangles on the ceiling in Figure 1 are supplied air exits and air exhausts, respectively.

The boundary conditions are set according to the actual site measurement and heat load estimation is referred to ASHRAE Handbook Fundamentals [6]. The air flow rates are measured by using a TSI 8372 ACCUBALANCE PLUS flow rate meter. There are 36 temperature sensors installed along the storage ring tunnel and the collected data are transmitted to our archive system. The boundary conditions of the real case, named as case 0, are listed in Table 1.

Table 1: Boundary conditions for the simulation case 0.

	Assumed condition	Set value
air exit	velocity inlet	1.49 m/s,22.12 ^{o}C
air exhaust	pressure outlet	0 Pa
cable tray	wall	882.59 W/m^3
magnets	wall	964.38 W/m^3
side wall	wall	Adiabatic

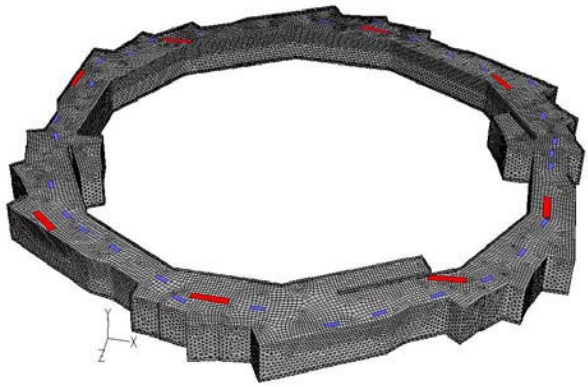

Figure 1: Grid structure of the simulated model.

As to the convergence criterion of the simulation, the residual value, i.e., the difference between values of next two iterations is set as 1×10^{-6} for all physical parameters.

SIMULATED RESULTS AND DISCUSSION

The temperature distribution in the storage ring tunnel is simulated. The simulated isotherm diagram of case 0 along the storage ring tunnel at the height of 1350mm, in which the beam orbit passes through, is shown in Figure 2. The temperature at the interface of the magnets is shown higher than adjacent area. The high temperature gradient area is near the magnets and cable trays, in which spatial temperature variation is about ±2.5 °C. On the other hand, the low temperature gradient area is near supplied air exits and air exhausts, in which spatial temperature variation is about ±0.2 °C.

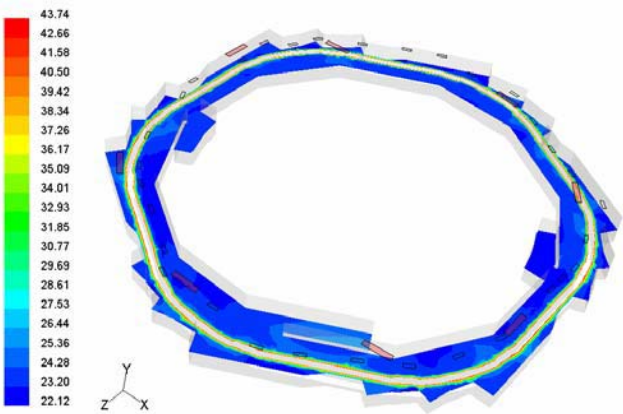

Figure 2: Isotherm diagram along the storage ring tunnel at the height of 1350mm of case 0.

The simulated temperatures of case 0 at 36 locations where 36 temperature sensors installed are compared with real collected data, and the compared results are illustrated in Figure 3. The results show that the average temperature difference is about 1.3 °C. Because the simulated results are close to the real case, we perform another two modified simulated cases, named as case 1 and case 2, respectively. The only differences among these cases are the boundary conditions at the supplied air exits, which are listed in Table 2.

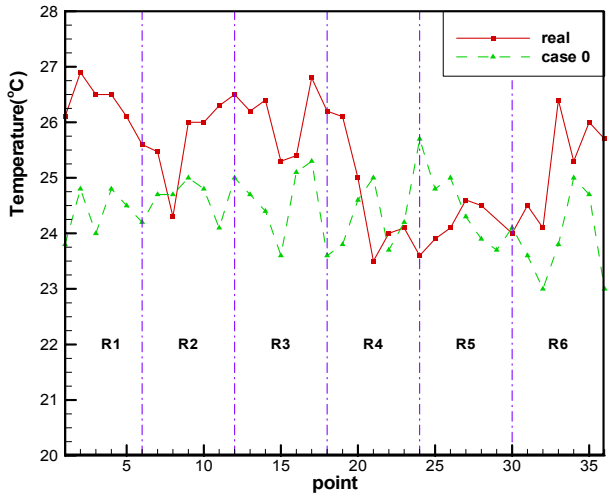

Figure 3: Comparison of the simulated and real measured temperatures at 36 locations.

Table 2: Boundary conditions at the supplied air exit for the simulation case 0, case 1 and case 2.

	Flow rate and temperature at air exits
Case 0	1.49 m/s, 22.12 °C
Case 1	2.50 m/s, 22.12 °C
Case 2	2.50 m/s, 20.0 °C

Figures 4 and 5 show the simulated stream lines near one air exhaust of case 0 and case 1, respectively. Two figures show similar flow field. The average flow velocity of case 1 is larger and accordingly the air exchange rate is higher. However, we can observe that there forms air shortcut between supplied air exits and the air exhaust in both cases. The shortcut shall decrease the cooling efficiency and cause the thermal non-uniformity. In case 1, we try to increase the supplied air velocity to improve the thermal non-uniformity phenomenon. Nevertheless, the improvement is not clear. Therefore, we not only increase the supplied air velocity but also decrease the air temperature in case 2.

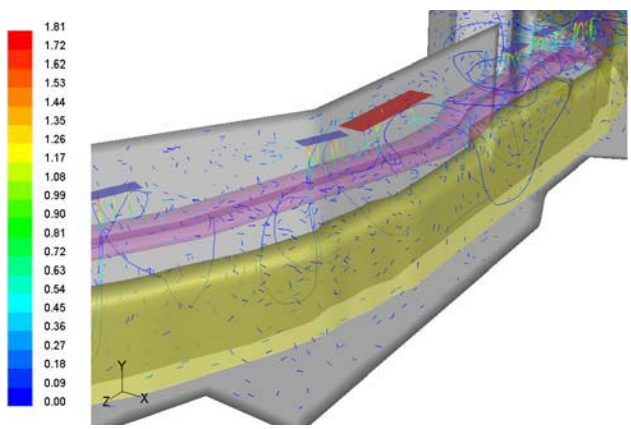

Figure 4: Stream lines near one air exhaust of case 0.

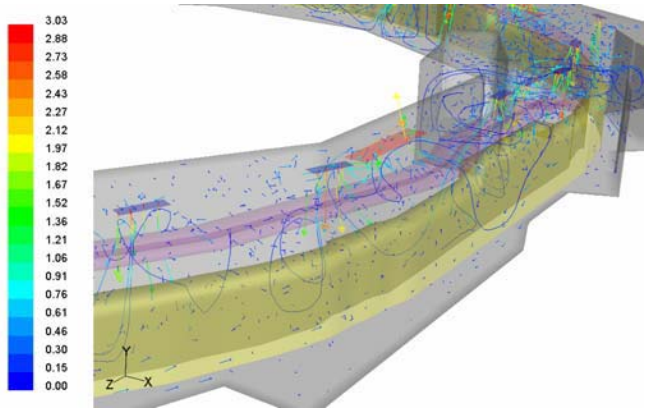

Figure 5: Stream lines near one air exhaust of case 1.

Figures 6 and 7 illustrate the simulated cross sectional stream lines and isotherm diagram of case 0 and case 2, respectively. Because the supplied air velocity in the case 1 is the same as that in the case 2, the stream lines are also similar in both cases.

There is a flow circulation in left side in both Figures 6 and 7. Because the supplied air velocity is larger in case2, the flow circulation tends to move down and in Figure 7. Furthermore, cooler supplied air can more clearly cool down the magnets and air temperature nearby. However, the cooling capacity will also be increased from 45.67 kW in case 0 to 133.11 kW in case 2.

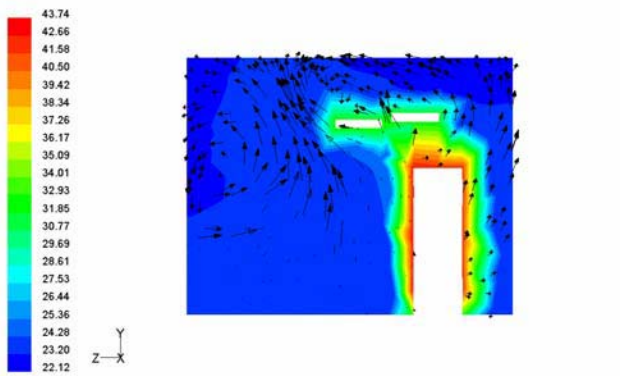

Figure 6: Cross sectional stream lines and isotherm diagram of case 0.

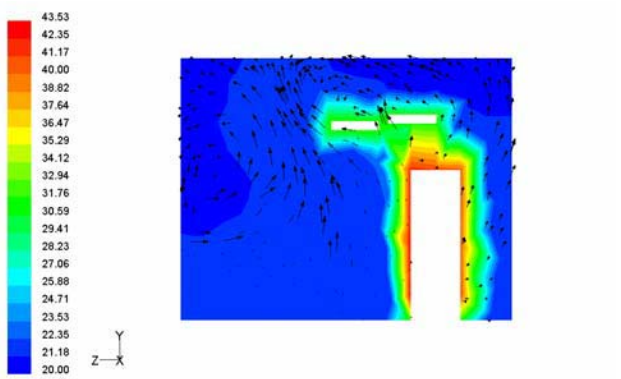

Figure 7: Cross sectional stream lines and isotherm diagram of case 2.

CONCLUSION AND FUTURE WORK

We have simulated the flow field and temperature distribution of the storage ring tunnel in this paper. Two improvement cases, i.e., cases 1 and 2, are also proposed and simulated. Simulated results show the supplied air shortcut forming between the supplied air exit and air exhaust.

Although the air temperature variation along the time in the storage ring tunnel has been controlled within $\pm 0.1^{o}C$, the spatial thermal uniformity still needs to be improved. More precise simulation is also needed to improve the AC system. Therefore, our future works are concluded as follows:

1. An AC system with larger cooling capacity is required to increase the supplied air flow rate and enhance the thermal uniformity.
2. Supplied air direction has to be modified to avoid the supplied air shortcut phenomenon.
3. We will perform transient CFD simulation to check the variations of temperature and flow field with time.
4. The models of the magnets, chambers, and cable trays have to be set up more precisely to decrease the simulation error.

REFERENCES

[1] J.R. Chen, H.M. Cheng, Z.D. Tsai, C.R. Chen, T.F. Lin, G.Y. Hsiung, and Y.S. Hong, "The Correlation between the Beam Orbit stability and the Utilities at SRRC", Proc. of 6th European Particle and Accelerator Conference EPAC98, Stockholm, Sweden, June 22-26, 1998.

[2] J.R. Chen, D.J. Wang, Z.D. Tsai, C.K. Kian, S.C. Ho, and J.C. Chang, "Mechanical Stability Studies at the Taiwan Light Source", 2nd Int'l Workshop on Mechanical Engineering Design of Synchrotron Radiation Equipment and Instrumentation (MEDSI02), APS, U.S.A., Sep 5-6, 2002.

[3] J.C. Chang, C.Y. Liu, and J.R. Chen, "Air Temperature Control Improvement for the Storage Ring Tunnel" 2003 Particle and Accelerator Conference (PAC), May 12-16, 2003, Portland, USA.

[4] D.S. Lee, Z.D. Tsai, J.R. Chen and C. R. Chen, "Cooling Air Flow Induced Thermal Deformation of the Magnet Lattice Girder", Proceedings of European Particle Accelerator Conference EPAC2000, Vienna, Austria, June 26-30, 2000.

[5] J.C. Chang, M. T. Ke, C.Y. Liu, and J.R. Chen, "Air Temperature Analysis and Control Improvement for the Large-Scale Experimental Hall" 2004 Asian Particle and Accelerator Conference (APAC), March 22-26, 2004, Gyeongiu, Korea.

[6] ASHRAE Handbook, Fundamentals, Chapter 28, 2001

